Design of a precision cryogenic rotary stage for optic or mask selection for the SCALES instrument mounted to the Keck 2 Telescope

C. Ratliff[a], N. MacDonald[a], J. Cabak[a], W. Deich[a], D. Sandford[a], M. Gonzales[a], A. Skemer[a], S. Sallum[a], D. Stelter[a], A. Hunter[a], R. Kupke[a], D. Dillon[a], D. Marques[a], C. Rodriguez, M. Savage[a], M. Kassis[b], J. Lyke[b], A. Hasan[c]
[a]UC Observatories, University of California, Santa Cruz, 1156 High St. Santa Cruz, CA 95064 USA
[b]W.M. Keck Observatory, 65-1120 Mamalahoa Highway, Kamuela, HI 96743 USA
[c]Indian Institute of Astrophysics, Koramangala, Bengaluru 560034, India

ABSTRACT

The SCALES instrument being developed at UC Observatories is designed to take spectra of directly imaged exoplanets in the thermal infrared (1-5 microns). The ability to switch from science imaging mode to pupil imaging mode to taking spectra at specific wavelengths requires precision mechanical subsystems to enable these different modes of operation at cryogenic temperatures. In this paper we discuss the design of a rotary stage that can position different Lyot masks, as well as different high precision metal optics to enable some of the broad functionality of SCALES. We will also review some of the analysis involved with validating the design, and specifics pertaining to the design of the precision mirrors mounted to this stage.

Keywords: cryogenic stage, opto-mechanical design, opto-mechanical alignment, optical mounting, aluminum cryogenic mirror, IR instrumentation, cryogenic spectrograph, Keck Telescope

1. INTRODUCTION

SCALES is a new instrument that will be mounted on the Keck 2 Telescope just downstream of the Keck 2 AO system. SCALES is designed to take spectra of directly imaged exoplanets at multiple wavelengths in the thermal infrared (1-5 microns). The ability to switch from science imaging mode to pupil imaging mode to taking spectra for specific wavelengths requires precision mechanical subsystems to enable these different modes of operation at cryogenic temperatures (-200C). In this paper we discuss the design of a rotary stage that can position different Lyot masks, as well as different high precision metal optics to enable some of the broad functionality of SCALES. Henceforth we will refer to this rotary stage as the Lyot mechanism. We will also discuss the design and analysis of the optics mounted to the Lyot mechanism, as well as thermal analysis and testing of the stepper motor drive system.

2. REQUIREMENTS OF DESIGN AND FUNCTIONAL DESCRIPTION

The primary functional requirement of the Lyot mechanism is to present either a mask or one of two different mirror optics into the center of the optical path of SCALES, enabling different modes of operation. There are several different Lyot masks with different degrees of over-coverage of the pupil. The key function of a Lyot mask is to eliminate diffraction and reflection of stray light incident on telescope hardware adjacent to the science light. The first mirror is a flat mirror that is used for imaging the science target and hence has demanding surface figure requirements. The second mirror is a toroid concave mirror that allows telescope pupil alignment to both the rotating cold stop and Lyot stop. The figure and positioning requirements on this mirror are similar but less demanding than the flat.

Table 1 outlines the main requirements for each Lyot mechanism optic/mask within SCALES. It should be noted that these requirements need to be met both at room temperature and at -200 C. Two of the more difficult requirements to meet are reliable positioning of each optic down to 70 microns (21 microns desired) and also maintaining the figure requirement of 35 nm RMS wavefront error on the flat mirror. This latter topic will be addressed in a later section of the paper.

Advances in Optical and Mechanical Technologies for Telescopes and Instrumentation VI,
edited by Ramón Navarro, Ralf Jedamzik, Proc. of SPIE Vol. 13100, 131006X
 · 0277-786X · doi: 10.1117/12.3020421

Table 1: SCALES Lyot mechanism functional requirements

Optical Component	Functional Requirements
Lyot Mask 1	A) Mask flare/diffraction from telescope hardware/entrance pupil B) Position accuracy in science beam to within 70 microns (required), 21 microns (desired) C) Position to within 1mm along optical axis D) Position repeatability <<70 microns E) Angular repeatability about optical axis <0.1 degrees F) adjustment precision in x-y plate <3.5 microns
Lyot Mask 2 thru 9	Similar position requirements (or less demanding) than Mask 1, allow for 8 different mask versions with different/larger amounts of pupil coverage
Flat science target imaging mirror	A) Maintain surface figure <35 nm RMS B) Surface roughness <5nm C) Allow for mirror manufacturing error of 24 nm RMS D) Angular position repeatability +/-0.01 degrees E) Must mount to less precise wheel surface (flatness~23 microns, worst case total of 48 microns) F) Position accuracy in x-y plane <100 microns G) Z positioning accuracy: NA (~1mm) H) Rotation error allowance about x and y axes +/-0.02 degrees I) Rotation error allowance about z axis allowance +/-0.05 degrees
Toroid pupil imaging mirror	Similar or less demanding that flat mirror
Requirements common to all optics	A) Insert any optic or mask into beam in less than 1 minute B) Provide a clear aperture for no mask and spots for mounting 11 optics/masks total C) Provide a transparent target for alignment D) Work reliably at room temperature and -200C E) Work at both ambient and high vacuum levels (10^{-6} Torr) F) Surface temperature rise of less than 20C with a time constant of less than a few minutes (for drive motor) G) No power dissipation to maintain position H) Athermal alignment behavior I) Maintain angular positioning warm and cold, athermal

Figure 1 shows the Lyot mechanism within the SCALES instrument with the optical axis highlighted in blue. In this configuration of the CAD, we show the optical axis ray highlighted in blue for both the science target imaging mode and pupil imaging mode.

The light comes in the entrance window and goes to the first fold mirror and then the second mirror which is an off axis asphere mirror. The asphere mirror sends the light through the cold stop, and then goes through an optical bandpass filter to the coronagraph/phase mask exchanger mechanism. At the next pupil plane is the Lyot mechanism. Downstream of the Lyot mechanism is a high precision tip tilt alignment mirror, and everything downstream of this assembly primarily functions to spatially slice the beam and create spectra.

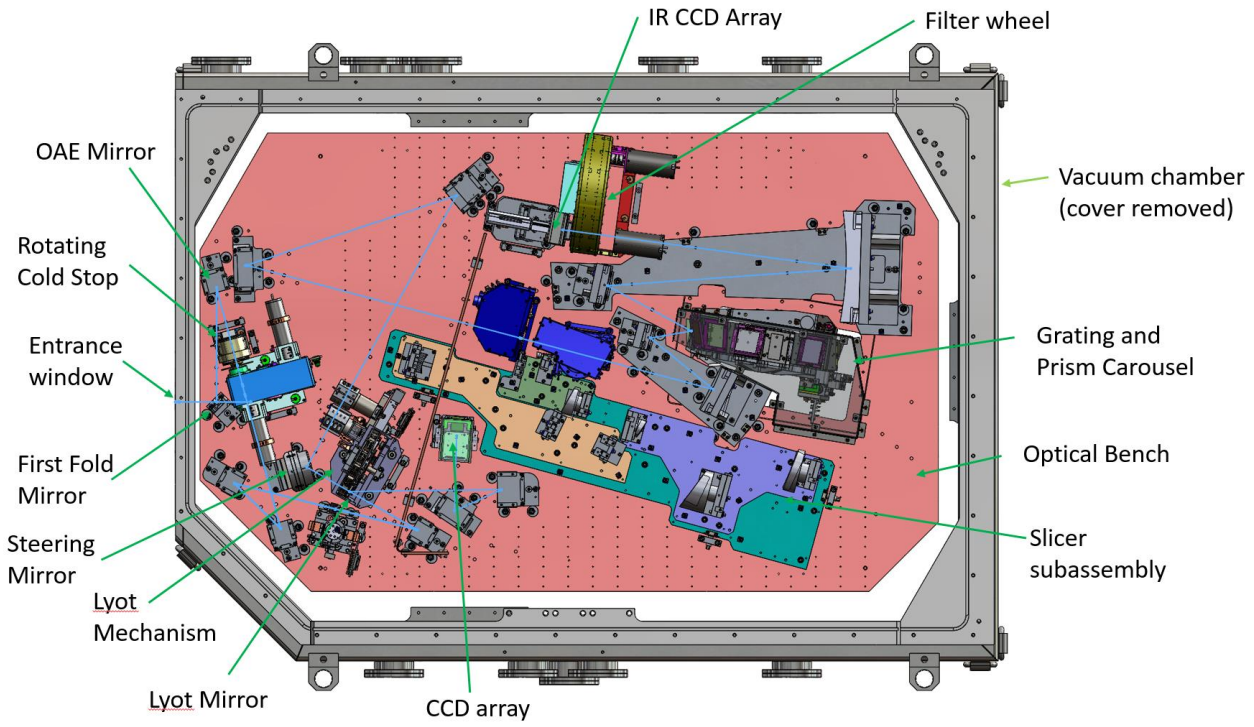

Figure 1: SCALES Instrument (cover removed)

2.1 Overview of the Lyot mechanism design

Figures 2 and 3 show CAD images of the of the Lyot mechanism. The aluminum support frame of the system is transparent to better show the design features. The frame, wheel and other parts are made of 6061 T651 aluminum. The use of 6061 aluminum alloy is typical throughout the SCALES design to make the system athermal both mechanically and optically. This feature allows us to align at room temperature and maintain that alignment after pumping down the enclosure to a pressure of approximately 10^{-6} Torr and then cooling to -200C. All of the non-transmission mirror optics are made of single point diamond turned RSA 6061 aluminum, the main optical bench is also made of 6061 aluminum.

Through the transparent Lyot mechanism support frame we can see that all of the optical elements are mounted to the main wheel. This wheel is moved to the appropriate optic using a Phytron cryo-prepared stepper motor along with a gear train. The gear train requires roughly 80 microns of backlash for each gear. Since there are five gears sized into our system to meet space, power, torque and timing requirements, we have a position uncertainty using the stepper motor and gears in excess of 200 microns. The precise positioning is achieved with a kinematic detent mechanism. This mechanism allows reliable high precision positioning with no heat dissipation. The wheel has 16 v-blocks along its outer circumference. Each v-block corresponds to a mask or optic position. A spherical roller engages with a v-block to the define position kinematically. The spherical roller and hybrid bearings within it are made of 440C stainless steel and silicon nitride. The Hertzian contact forces are high on these items which require the use of hard materials. Although these parts are not 6061 aluminum, the overall aluminum structure still defines their position within the assembly, maintaining athermal characteristics. The pivot of the lever arm on which the spherical roller is mounted is made out of 400 series stainless steel. This flexure is made by C-Flex Bearing (model number: JD-10). This C-flex bearing is essentially frictionless and highly repeatable.

The bearings supporting the gear axles are located by pockets that are CNC machined into the main support frame and panels. The panels align to the main frame using two precision ground pins per panel to locate the bearing pockets to within 25 microns.

The Lyot mechanism spherical detent can be engaged either passively or actively with a detent engage/release mechanism. We are not sure which mode of operation we will pursue for the final design. It appears that the passive approach can meet requirements, but may not prove as robust in the long run. The main advantage of the active detent approach is that better accuracies are easier to achieve, typically less than 13 microns. In the active mode of engaging the spherical detent, we use a gearhead Phytron stepper motor with a cam follower attached to the gearhead axle. A spring with approximately 8 lbs of force then pulls on the end of the lever arm where the spherical detent is mounted. The force is high enough to overcome the inherent resisting torque within the gear driving stepper motor. We are in the stage of preliminary testing of each mode.

Figure 4 shows an exploded view of the Lyot mechanism wheel. The wheel turns on two axle bearings. These wheel bearings use silicon nitride balls and are coated with tungsten disulfide solid lubricant. The bearing pockets in the wheel that hold the bearings are a mild interference fit and consist of flexure fingers machined into the wheel itself. The flexure fingers reduce the load on the 440 C stainless steel bearing races as the temperature goes to -200C.

Each optic/mask is precisely placed on the Lyot wheel with two precision ground stainless steel pins. The position of the whole Lyot mechanism is precisely placed on the optical bench with two pins as well, and this position relative to the science light can be verified with an alignment reticle and an autocollimation mirror that are also mounted to the Lyot wheel.

The wheel position is sensed with a magnet wheel attached to the main Lyot wheel. A series of 17 counterbores are machined into the magnet wheel where 17 cylindrical neodymium magnets are epoxied with 3M 2216 epoxy. This epoxy has been used successfully by a number of other cryogenic instruments which is why it was selected here. The counter-bores help ensure a consistent 600 micron gap between the face of the magnets and the stationary Hall effect sensors mounted to a printed circuit board that is attached to the main frame. Figure 5 shows the magnet wheel and Hall sensors. There are two Hall Asahi HG-106A sensors side by side to allow us to sense direction. University of California Observatories is presenting another SPIE paper at this symposium that goes into details about the sensing precision and electronic details of the design.

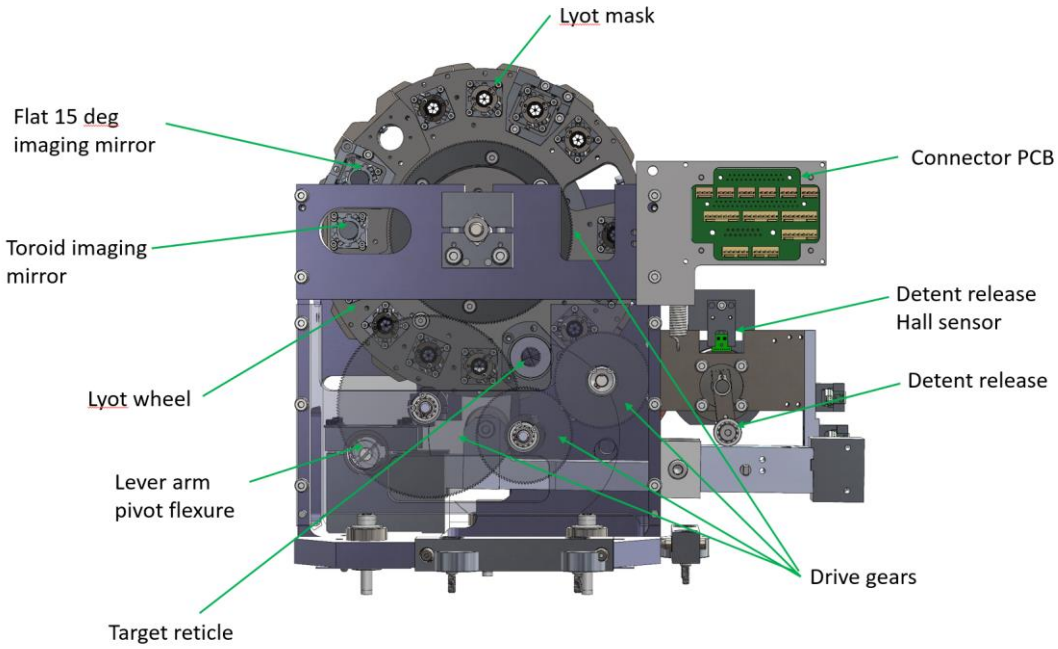

Figure 2: The Lyot mechanism showing the masks and optics it can swap into the telescope beam

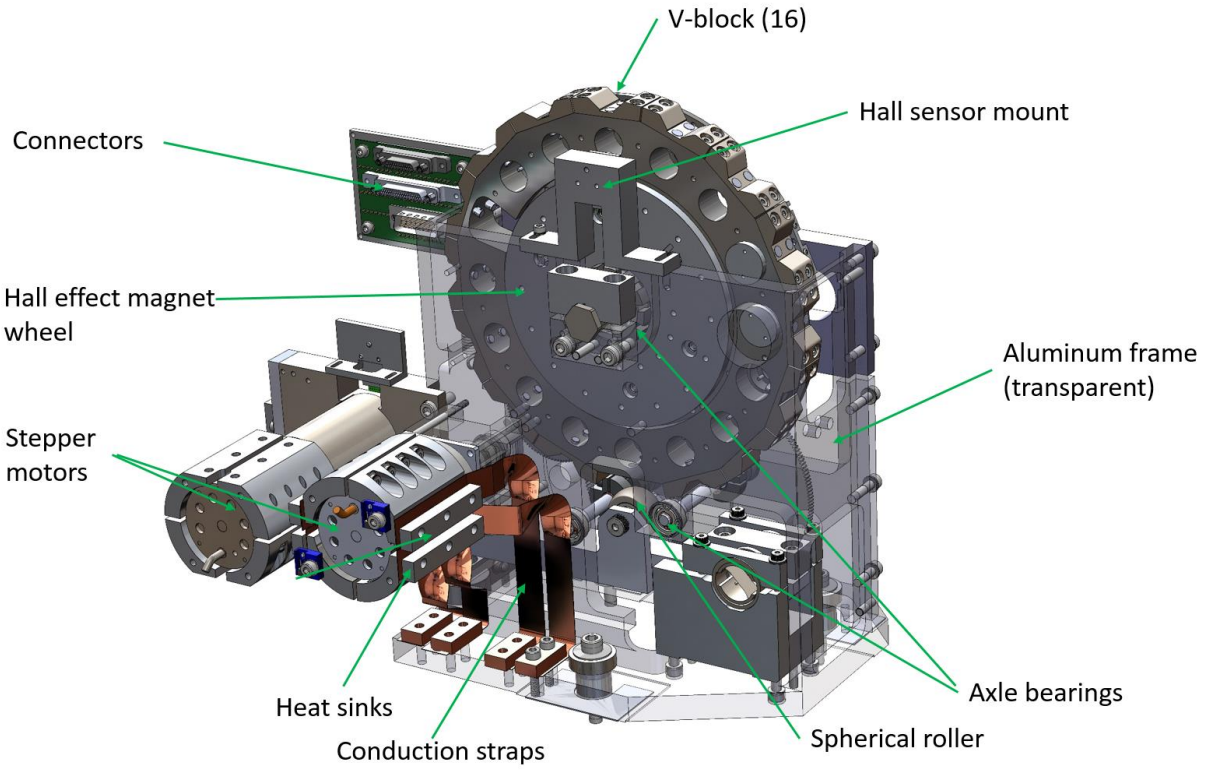

Figure 3: The motor side of the Lyot mechanism

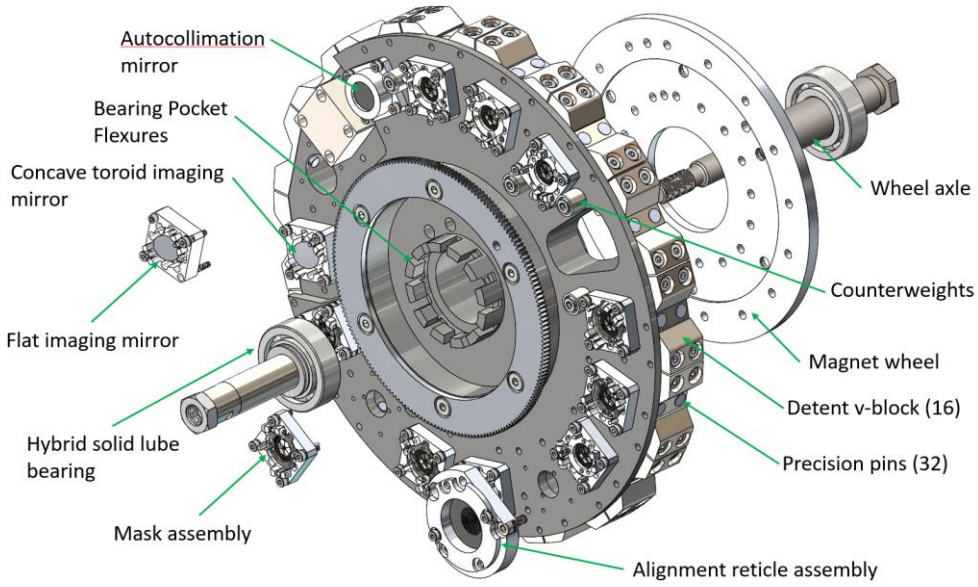

Figure 4: Exploded view of the Lyot wheel

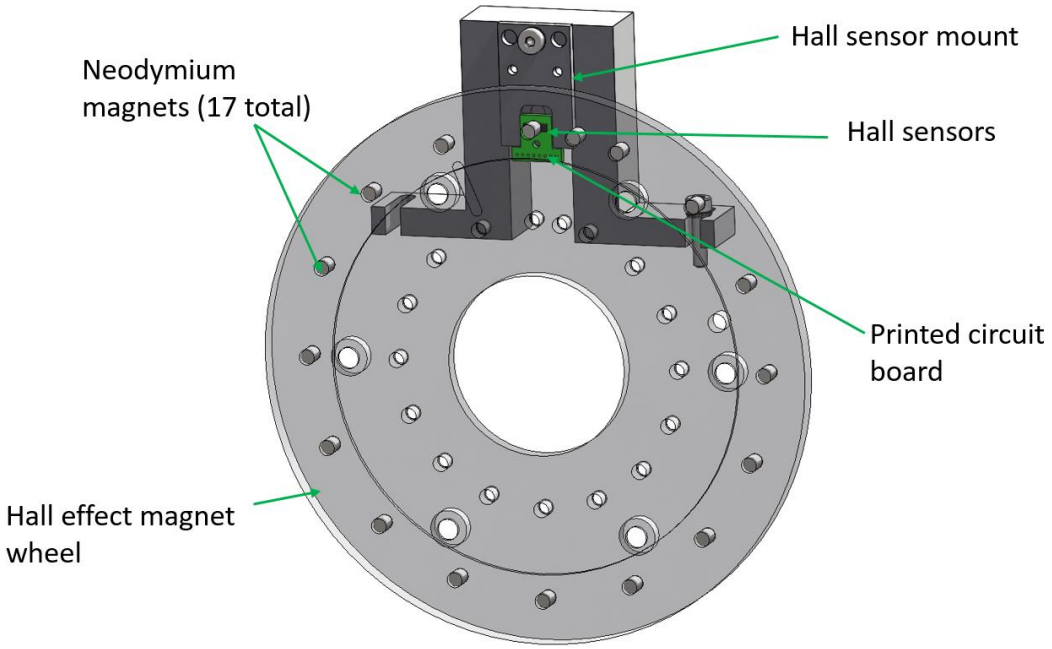

Figure 5: View of the Hall effect sensor assembly

3. MIRROR DESIGN

The requirements for the imaging mirror are given in Table 1. Of these requirements, there are two that figured into the design considerably. The maximum surface figure error of 35 nm RMS is challenging. Given that the manufacturing for the mirror allowed an error of 24 nm RMS, we have an allowance of 11nm RMS induced optical surface deformation when fastening it to the wheel surface. Figure 5 shows a close up of the optic mounted to the wheel. The tolerance of the flatness on the wheel in this area is 23 microns, and the tolerance on the flatness of the backside of the optic that mounts to the wheel surface is assumed to be 25 microns. So the worst case clamped distortion of the mounting side of the mirror is 48 microns. One means of attaching optics to imperfect surfaces such as this is to use flexures. Using epoxy or silicone was not an option due to the high vacuum levels, large temperature swings and large differences in coefficient of thermal expansion. However, there were a number of different aluminum flexure geometry options that could potentially work in this application. The design that was settled on is shown in Figure 6 which is a diaphragm type flexure connecting a clamp feature and a SPDT optic in a single part. We came up with this design because it allowed almost all of the machining to be done on a single CNC lathe setup. The optic was designed by UC Observatories, and Son-x fabricated the optics with their SPDT technology. The material used is RSA 6061 aluminum due to its low internal stress levels that result in less deformation during machining. All of the materials contacting the optic (wheel and clamp) are also 6061 aluminum.

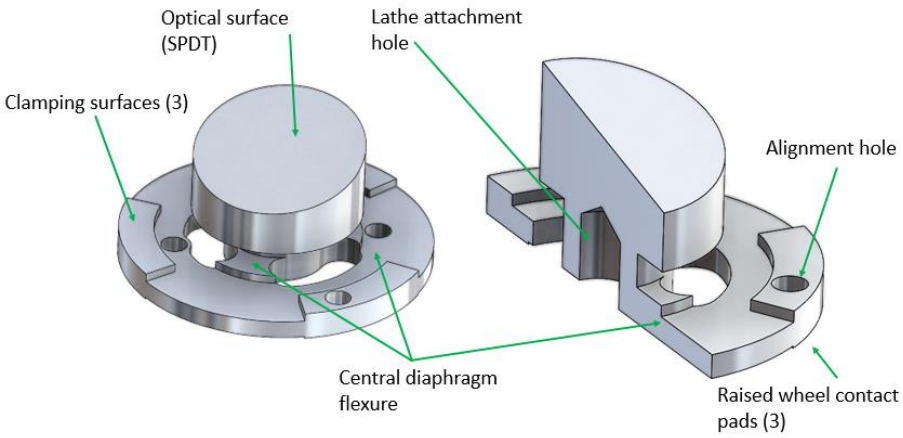

Figure 6: A SPDT optic mounted to the Lyot mechanism

3.1 Deformation analysis

Finite element analysis (FEA) was used to estimate the resulting optical surface distortion for a worst case scenario. We used FEA to both iterate and eventually validate the final design of the diaphragm flexure. The key assumptions for this analysis are that there is a sum of 48 microns of non-flatness in both the Lyot wheel surface and the mirror mating surface (worst case). It is also assumed that the clamping surfaces are fully pressed against the mating wheel surface.

The main variables that we changed to optimize the design for both mirror figure and ease of handling and manufacturability are shown in Figure 7. D1, D2 and D3 on this figure were the main variables of interest. We also tried three separated flexures (pie slicing the diaphragm), and with our geometry limitations, this alternative worked well for mirror figure, but proved too delicate for easy manufacturing. The results for this FEA are shown in Figure 8. Figure 9 shows the final design FEA results. It should be noted that peak to valley deformation from a planar surface for the final design was 6 nanometers. If the mirror fabricators use up their full 24nm RMS budget, we will still meet requirements. However, it should be noted that a shim will need to be applied to eliminate excessive tilt error, in the case of this analysis the resulting tilt error is 0.06 degrees.

A Zygo interferometer will be used to verify the final figure of the flat mirror optic.

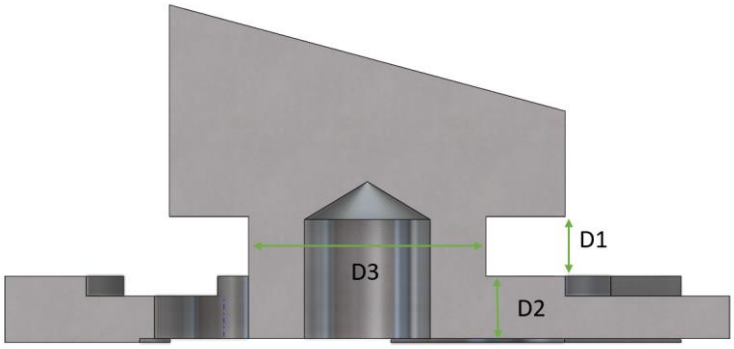

Figure 7: Variables to optimize optic design

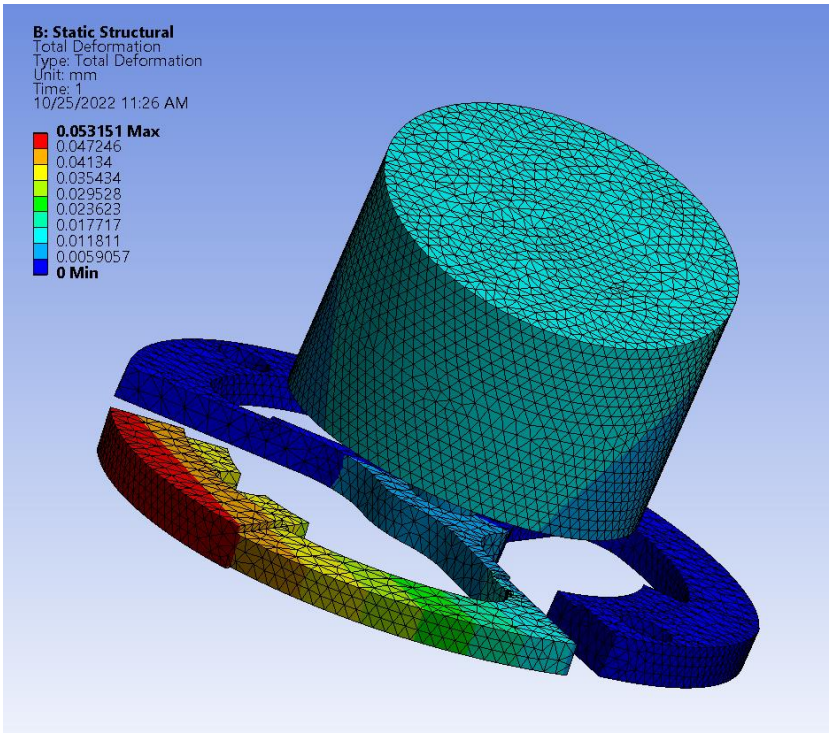

Figure 8: Three leg flexure design FEA results (too delicate)

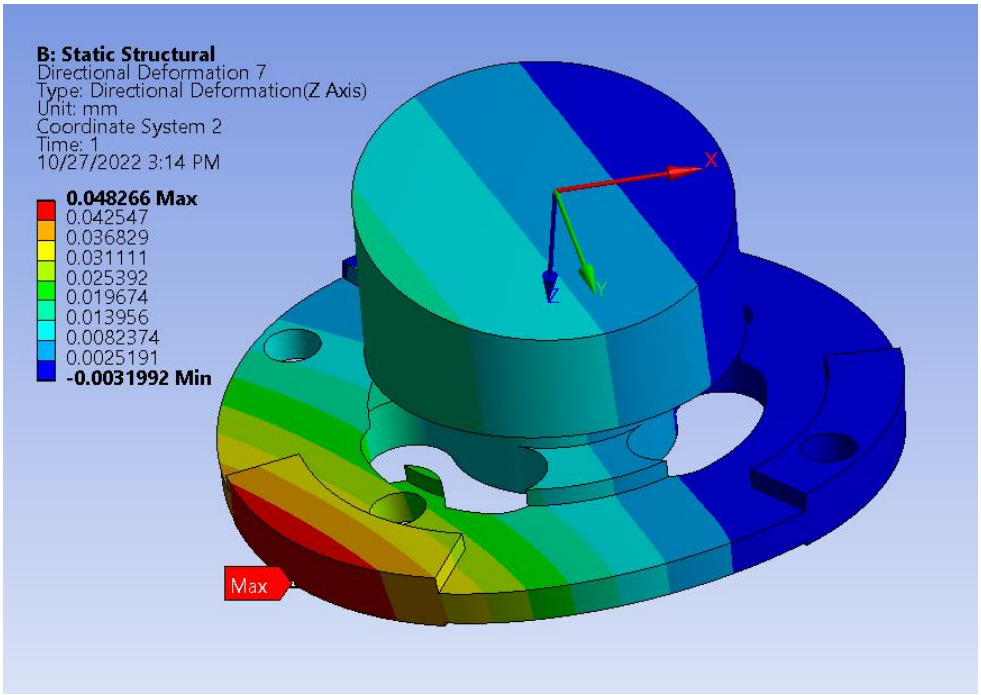

Figure 9: Final design FEA results, added error of 4.3 nm Peak to Valley (after subtraction of tilt error)

4. THERMAL ANALYSIS

The temperature rise of the stepper motors is an important matter in keeping background IR to a minimum for exoplanet imaging. The requirement is that no surface within the enclosure rise more than 20 C above the bench temperature. It should also be noted that we want to minimize temperature non-uniformity within each subassembly to maintain consistent relative positions of components (like gears and bearings) due to the thermal expansion coefficient of 6061 aluminum. The final reason temperature rise is important is due to limitations of the stepper motors in a vacuum. The heat dissipation of the stepper motor windings is more limited in high vacuum due to the lack of convection. The vacuum stepper motors we are using are limited to half of their atmospheric pressure current levels by the manufacturer. We typically only run the motors at ambient temperature and pressure or at cryogenic temperatures under vacuum, but not under vacuum and ambient temperatures. The analysis discussed in this section addresses keeping the peak surface temperature rise under 20C since that is what is potentially exposed to the science light. We do not address the temperature rise within the stepper motor windings internal to the motor.

Finite element analysis (FEA) was performed to estimate the temperature rise of the stepper motor for different heat sinking conditions and different duty cycle conditions. The first analysis that was done had the stepper motor running continuously at a power of 4.25 Watts (100% duty cycle) and mounted to the Lyot mechanism frame and motor mount. Even in this configuration without an additional heat sink, there is significant conduction through the motor mount and frame into the actively cooled optical bench.

The main assumptions for this analysis are 4.25 Watts of power being generated uniformly in the exterior motor housing that holds the windings. The Phytron stepper motor material is 303 stainless steel, while the motor mount and frame are made of 6061 aluminum. All of the material properties are temperature dependent based on the NIST cryogenic material property curves. This analysis also accounts for the thermal resistance between mating parts which contributes significantly to the maximum temperature rise. The thermal conductance value for the stainless steel to stainless steel interfaces is assumed to be 1800 $W/m^2°C$, and this interface proved to be a significant thermal resistance. For this first case, the temperature rise results are given in Figure 10 showing that the steady state temperature rise is 55C, higher than our requirements allow.

There was iteration with the design, and for the final design we expect to use a copper heat sink, conduction strap and an aluminum motor enclosure. The result for this situation along with a duty cycle of 100% are given in Figure 11. The external surface temperature rise here is 6.4C and the motor temperature rise is ~35 C. If we limit the duty cycle to 10%, the resulting external surface temperature rise is less than 1C.

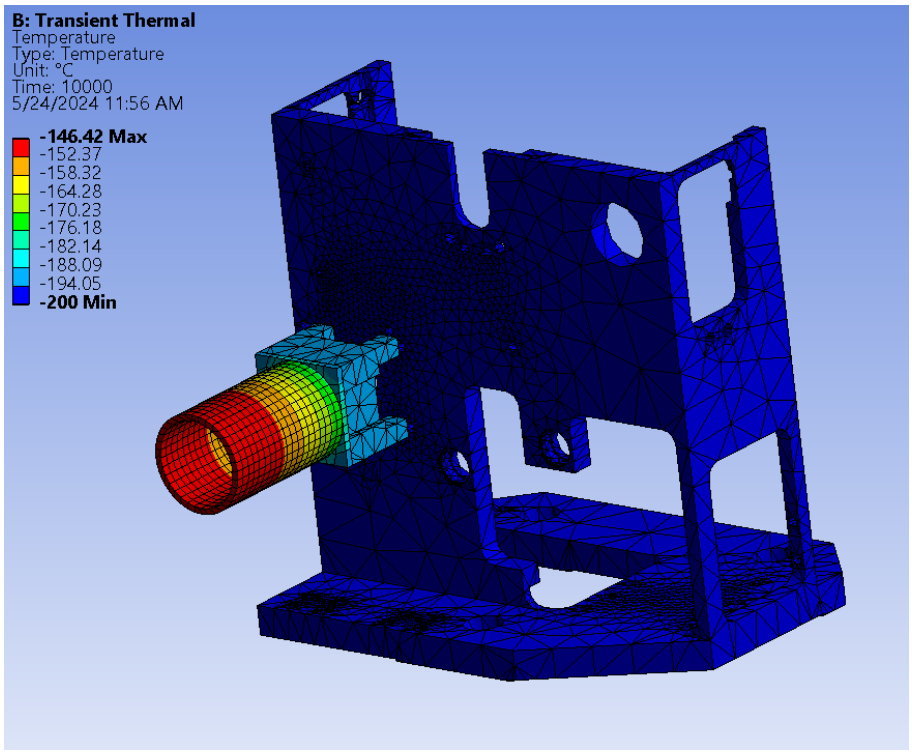

Figure 10: Temperature rise of stepper motor (54C)

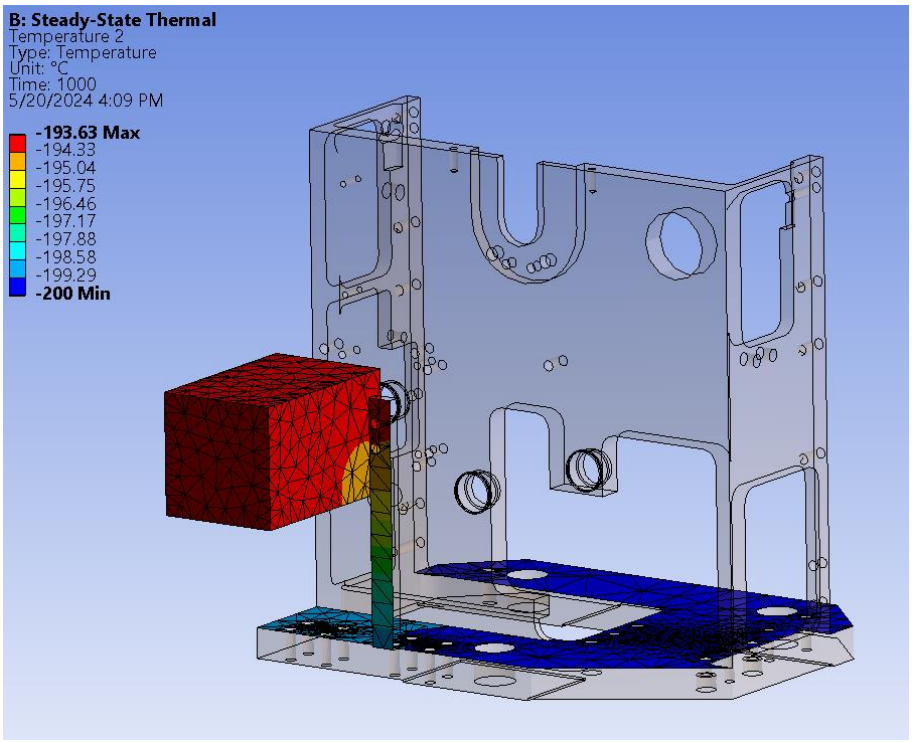

Figure 11: Temperature rise with heat sink and motor cover

5. CONCLUSION

In conclusion, we have discussed some of the interesting topics regarding the design of the SCALES Lyot mechanism. The goal of the SCALES instrument is to both image and take spectra of exoplanets on the Keck 2 Telescope. The Lyot mechanism is still in the process of preliminary testing, but looks to be capable of meeting requirements. This mechanism is essential to reducing stray light as well as enabling imaging and beam alignment. So far, it looks like it can meet position repeatability requirements with either an active or passive detent system. I expect that if our requirements get tighter for a Lyot mask with less overlap of the pupil (more science light), the active detent mode will provide better accuracy and long term repeatability.

In designing, fabricating and building this cryogenic stage there are some important points to mention:

1. The design should include feedback mechanisms where possible (cameras, encoders, etc.), for testing diagnostic purposes. It takes much time for cooling down and warming up cryogenic mechanisms. Faster diagnostics can speed cycles of learning. Visibility within cryogenic vacuum chambers is very limited and sometimes it is difficult to diagnose what is happening if there is a problem. In-situ observability is very nice to have and sometimes essential. Encoders and feedback sensors that are cryogenically capable are quite limited.
2. Since cycles of learning for cryogenic mechanisms are slower than non-cryogenic, more up front time spent on the design in making it more robust and reliable is important. This time investment will usually pay off with reduced testing and retesting/redesign of less reliable designs.
3. Use stress relieved material where dimensional stability is required (T651 or RSA 6061 aluminum).
4. Motors heat up much more quickly in high vacuum. Typically, conduction heat sinks are required unless duty cycles are very low. Convection heat losses do not exist, and radiation is usually not sufficient to cool a motor or other heat generating devices.
5. We will conduct more tests to verify we can meet all of the requirements over the life span of the Lyot mechanism.

ACKNOWLEDGEMENTS

We gratefully acknowledge the support of the SCALES collaborating institutions. These institutions include: the University of California Observatories, W.M. Keck Observatory, the IR lab group at UCLA, and the group at India Institute of Astronomy for optical and mechanical collaboration. We would also like to thank NAOJ for their information on their IRIS stages. I would also like to thank Andy Skemer for initiating this project and acting as PI of it. This work was also supported by the Heising-Simons Foundation, to whom we are also grateful. I would also like to thank Monica Ratliff for her editing of this paper.

REFERENCES

[1] Stelter R. et al., “Update on the preliminary design of SCALES: The Santa Cruz Array of Lenslets for Exoplanet Spectroscopy”, Proceedings of SPIE Vol. 11447, (2020)
[2] Marquardt E. et al., “Cryogenic material properties database”, 11th International Cryocooler Conference, (2000)
[3] Uraguchi F. et al., “The Infrared Imaging Spectrograph (IRIS) for TMT: Prototyping of cryogenic compatible stage for the Imager”, Proceedings of SPIE Vol. 9908, (2016)
[4] Krause O. et al., “Wheel mechanisms of the mid-infrared instrument aboard the James Webb Space Telescope – Performance of the flight models”, Proceedings of the 13th European Space Mechanisms and Tribology Symposium, ESA SP-670, (2009)
[5] Fletcher L. et al., [Heat Transfer Between Surfaces in Contact: An Analytic and Experimental Study of Thermal Contact Resistance of Metallic Interfaces], Arizona State University, Tempe, AZ, 82-86, Appendix A, (1968).